
Article:
Jin, L, Lee, R and Robertson, I (2015) Analysis and design of a dielectric insular image guide. Microwave and Optical Technology Letters, 57 (11). pp. 2465-2467. ISSN: 0895-2477

https://doi.org/10.1002/mop.29380

Analysis and Design of a Dielectric Insular Image Guide

Lukui Jin, Razak M. A. Lee and Ian Robertson

***Abstract*—In this paper, a detailed theoretical analysis of the dielectric insular image guide (DIIG) is presented to provide a solution for low-loss millimeter-wave (mm-wave) transmission lines. The effective dielectric constant (EDC) method is utilised to derive the characteristic equations and attenuation constants. A DIIG prototype in the Ka band is fabricated using a standard LTCC technique. Results from measurements agree well with theoretical calculations and simulations. A loss of 0.012 dB/mm at 35 GHz is achieved, which indicates great potential for further development to realise highly-integrated low-loss microwave components and systems.**

***Index Terms*—Millimeter wave circuits, transmission lines, multichip modules, Dielectric devices.**

I. Introduction

THE study of the dielectric guide (DG) started as early as 1910 when Hondros *et al*. analysed the propagation characteristics of electromagnetic waves along cylindrical DGs [1]. In 1952, King first proposed a large pure metallic layer at the bottom of the DG, which gives rise to a new configuration popularly referred to as the dielectric image guide (DIG). This enables the possible applications of the DG at the millimeter-waves (mm-waves) and proves to be the simplest dielectric integrated guide structure [1], [2].

In the search for a low-loss millimeter-wave transmission line, however, the DIG is not a perfect solution. The DIG suffers from conductor loss, with a large field concentration near the metallic ground plane when it's operating in the fundamental TM_{11}^{y} mode. This can be reduced by introducing a low-permittivity (normally lower than that of the DIG dielectric) low-loss dielectric layer between the DIG dielectric and the ground plane [3]. This layer works as an insulator which keeps the fields away from the ground plane and, hence, this alternative form of DIG is referred to as dielectric insular image guide (DIIG) [1].

To theoretically analyse the DG and its variations, Marcatili's paper [4] in 1969 is the earliest and most comprehensive effort to give a deep insight into the waveguiding mechanisms of the low-permittivity rectangular DG. In this paper, Marcatili introduced an approximate solution by neglecting the electromagnetic fields in certain regions. Based on that premise, Marcatili calculated the propagation constants and provided a solution for both a single and two coupled DGs in the form of transcendental equations, which is further approximated into a closed form. With the establishment of characteristic equations for this boundary value problem, it was then found that this DG model can be split into two independent and simpler slab guides with infinite extension along one single direction, respectively, $i.e.$, the horizontal and vertical slab guides [4].

In 1970, Knox *et al*. followed Marcatili's approximation and introduced an effective dielectric constant (EDC) method, which was applied to the DIG. Up until now, it is still the most commonly used method for analysing the propagation characteristics of the rectangular DIG [5]. Through the image theory, it can be inferred that DIG represents the top half of a rectangular DG of twice the height, except that certain modes are shorted out by the metallic ground plane and hence suppressed. This is a distinct advantage over the DG, giving a much wider frequency bandwidth for single mode operation [1].

Apart from these two approximate methods, rigorous methods have also been developed with the wide application of computers. Taking into account what's neglected in Marcatili's method and the EDC method, the accuracy has been improved, although the complexity has also been significantly increased. Research on this subject has given rise to the mode-matching method [6]–[8], the generalised telegrapher's equations [9] and the finite element iterative method [10], *etc*. All these numerical methods tolerate the existence of geometrical discontinuities which enable the coupling among different modes and create hybrid ones [11].

This paper focuses on the DIIG and presents detailed analysis in terms of the propagation characteristics using the EDC method in [5]. In Section II, the characteristic equations are given and the analytical expressions for the attenuation constant, α, and its constituents are also derived. Results from theoretical calculations are compared with the simulated ones from a commercial simulator, HFSS™, based on the FEM method in Section III. Finally, three DIIG prototypes working in Ka-band are fabricated using LTCC material and measured to verify the design in Section IV.

II. Theory

This section deals with the theoretical analysis of the TM_{mn}^{y} and TE_{mn}^{y} modes in the DIIG using the EDC method. Both the phase constant, β, and the attenuation constant, α, are derived.

As shown in Fig. 1(a), an insular layer with a low dielectric constant of ϵ_{r_2} and a thickness of $d/2$ is added below the original DIG dielectric (ϵ_{r_1}). Using the EDC method, the DIIG can be divided into three constituent regions each of which can be then extended into infinite horizontal slab guides. After the equivalent dielectric constants, ϵ_{re_1} and ϵ_{re_2} are extracted, the vertical slab guides can also be established in Fig. 1(b).

Manuscript received 09 June, 2014

L. Jin, and I. Robertson are both with the School of Electronic and Electrical Engineering, University of Leeds, Leeds, LS2 9JT, United Kingdom.

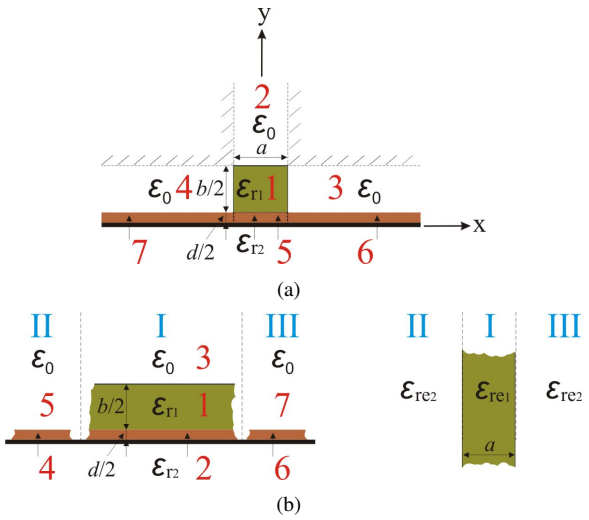

Fig. 1. The cross-sectional view of: (a) the DIIG, (b) equivalent horizontal and vertical slab guides for the EDC method.

A. TM^y_{mn} Mode

1) Characteristic equations: The DIIG is first extended into infinite horizontal slab guides, as shown in Fig. 1(b). Hence, the characteristic equations for the horizontal slab guides in the three regions are derived and given as:

$$1+\frac{k_{y2}}{\epsilon_{r2}k_{y3}}\tanh\left(k_{y2}d/2\right)-\frac{k_{y1}}{\epsilon_{r1}k_{y3}}\tan\left(k_{y1}b/2\right)+\frac{\epsilon_{r1}k_{y2}}{\epsilon_{r2}k_{y1}}\tanh\left(k_{y2}d/2\right)\tan\left(k_{y1}b/2\right)=0,\ \text{Region I} \quad (1a)$$

$$1-\frac{k_{y4}}{\epsilon_{r2}k_{y5}}\tan\left(k_{y4}d/2\right)=0,\ \text{Regions II \& III} \quad (1b)$$

where

$$\begin{aligned} k_{y1}&=\sqrt{\epsilon_{r1}k_0^2-\beta_{h1}^2}\\ k_{y2}&=\sqrt{(\epsilon_{r1}-\epsilon_{r2})k_0^2-k_{y1}^2}\\ k_{y3}&=\sqrt{(\epsilon_{r1}-1)k_0^2-k_{y1}^2}\\ k_{y4}&=\sqrt{\epsilon_{r2}k_0^2-\beta_{h2}^2}\\ k_{y5}&=\sqrt{(\epsilon_{r2}-1)k_0^2-k_{y4}^2} \end{aligned} \quad (2)$$

With k_{y1} and k_{y4} solved, Regions I, II, and III are then transformed into three uniformly-distributed media whose equivalent relative dielectric constants are

$$\begin{aligned} \epsilon_{re1}&=\epsilon_{r1}-\left(\frac{k_{y1}}{k_0}\right)^2\\ \epsilon_{re2}&=\epsilon_{r2}-\left(\frac{k_{y4}}{k_0}\right)^2 \end{aligned} \quad (3)$$

As a result, the infinite vertical slab guide is built up to obtain its characteristic equation as:

$$1+\frac{k_{x0}^2-k_{x1}^2}{k_{x0}k_{x1}}\tan\left(k_{x1}a/2\right)-\tan^2\left(k_{x1}a/2\right)=0 \quad (4)$$

which can then be split into

$$\begin{aligned} 1-\frac{k_{x1}}{k_{x0}}\tan\left(k_{x1}a/2\right)&=0, \quad \text{even mode}\\ 1+\frac{k_{x0}}{k_{x1}}\tan\left(k_{x1}a/2\right)&=0, \quad \text{odd mode} \end{aligned} \quad (5)$$

where

$$\begin{aligned} k_{x1}&=\sqrt{\epsilon_{re1}k_0^2-\beta^2}\\ k_{x0}&=\sqrt{(\epsilon_{re1}-\epsilon_{re2})k_0^2-k_{x1}^2} \end{aligned} \quad (6)$$

Note that β is the final phase constant of the DIIG.

It is also worth noting that the transendental equations, (1) and (4), have infinite roots. The TM^y_{mn} mode is determined by the mth root of k_{x1} through (4) and the nth root of k_{y1} through (1).

2) Field components: According to [4], [5], E_y and H_x are the dominating field components for the TM^y_{mn} mode. Furthermore, the wave behaviours in Areas 1, 2, 3, and 4 (shown in Fig. 1(a)) are the same as those in the DIG, *i.e.*, standing inside the dielectric, whereas decaying exponentially with distance outside it in the x and y directions. The fields in the insular layer, however, are different: for Area 5, the fields stand along the x direction and decay along the y direction; for Areas 6 and 7, the fields decay on both x and y directions extending toward infinity.

Since TM^y_{11} is the dominant mode in the single-mode frequency band and belongs to the even-mode family, only the field expressions of even TM^y_{mn} modes are given. Through the EDC method, the field expressions in those five areas shown in Fig. 1(a) are as follows: main electric field, E_y,

$$\begin{aligned} E_{y1}&=A_1\sqrt{\frac{\omega\mu\beta_{h1}}{k_{x1}k_{y1}}}\cos(k_{x1}x)\{\cos\left[k_{y1}(y-d')\right]+A_2\sin\left[k_{y1}(y-d')\right]\}\\ E_{y2}&=A_1A_3\sqrt{\frac{\omega\mu\beta_{h1}}{k_{x1}k_{y3}}}\cos(k_{x1}x)\mathrm{e}^{-k_{y3}\left[y-(b'+d')\right]}\\ E_{y3}&=A_1\sqrt{\frac{\omega\mu\beta_{h1}}{k_{x0}k_{y1}}}\sin(k_{x1}a')\{\cos\left[k_{y1}(y-d')\right]+A_2\sin\left[k_{y1}(y-d')\right]\}\mathrm{e}^{-k_{x0}(x-a')}\\ E_{y4}&=A_1\sqrt{\frac{\omega\mu\beta_{h1}}{k_{x0}k_{y1}}}\sin(k_{x1}a')\{\cos\left[k_{y1}(y-d')\right]+A_2\sin\left[k_{y1}(y-d')\right]\}\mathrm{e}^{k_{x0}(x+a')}\\ E_{y5}&=A_1A_4\sqrt{\frac{\omega\mu\beta_{h1}}{k_{x1}k_{y2}}}\cos(k_{x1}x)(\mathrm{e}^{k_{y_2}y}+\mathrm{e}^{-k_{y_2}y}), \quad -a'\le x\le a'\\ E_{y6}&=A_1A_4\sqrt{\frac{\omega\mu\beta_{h1}}{k_{x0}k_{y2}}}\sin(k_{x1}a')\mathrm{e}^{-k_{x0}(x-a')}(\mathrm{e}^{k_{y_2}y}+\mathrm{e}^{-k_{y_2}y}), \quad a'\le x\le\infty\\ E_{y7}&=A_1A_4\sqrt{\frac{\omega\mu\beta_{h1}}{k_{x0}k_{y2}}}\sin(k_{x1}a')\mathrm{e}^{k_{x0}(x+a')}(\mathrm{e}^{k_{y_2}y}+\mathrm{e}^{-k_{y_2}y}), \quad -\infty\le x\le -a' \end{aligned} \quad (7)$$

main magnetic field, H_x,

$$\begin{aligned} H_{x1} &= \sqrt{\frac{\epsilon_1\beta}{\mu\beta_{h1}}}E_{y1} \\ H_{xi} &= \sqrt{\frac{\epsilon_0\beta}{\mu\beta_{h1}}}E_{yi}, \quad i = 2,\ 3,\ 4 \\ H_{xj} &= \sqrt{\frac{\epsilon_2\beta}{\mu\beta_{h1}}}E_{yj}, \quad j = 5,\ 6,\ 7 \end{aligned} \tag{8}$$

where

$$\begin{aligned} A_2 &= \frac{k_{y1}\tan(k_{y1}b') - \epsilon_{r1}k_{y3}}{k_{y1} + \epsilon_{r1}k_{y3}\tan(k_{y1}b')} \\ A_3 &= \frac{\epsilon_{r1}k_{y3}}{k_{y1}\cos(k_{y1}b') + \epsilon_{r1}k_{y3}\sin(k_{y1}b')} \\ A_4 &= \frac{\epsilon_{r1}k_{y2}\mathrm{sech}(k_{y2}d')}{2\epsilon_{r2}k_{y1}} \\ a' &= a/2,\ b' = b/2,\ d' = d/2 \end{aligned} \tag{9}$$

3) Attenuation constant, α: Following the perturbation method in [12], the attenuation constant, α, of the DIIG is given by:

$$\alpha = \frac{P_l}{2P} = \frac{P_{lc} + P_{ld} + P_{lr}}{2P} = \alpha_c + \alpha_d + \alpha_r \tag{10}$$

where

$$\begin{aligned} P &= P_1 + P_2 + P_3 + P_4 + P_5 + P_6 + P_7 \\ P_{lc} &= P_{lc5} + P_{lc6} + P_{lc7} \\ P_{ld} &= P_{ld1} + P_{ld5} + P_{ld6} + P_{ld7} \\ P_{lr} &= P_2 + P_3 + P_4 \end{aligned}$$

Before α is derived through (10), the simplification parameters need to be defined as:

$$\begin{aligned} M_x &= \frac{k_{x1}a + \sin(k_{x1}a)}{k_{x1}^2} \\ N_x &= \frac{\sin^2(k_{x1}a/2)}{k_{x0}^2} \\ M_y &= \left\{(1 + A_2^2)k_{y1}b + (1 - A_2^2)\sin(k_{y1}b)\right. \\ &\quad \left. + 2A_2\left[1 - \cos(k_{y1}b)\right]\right\}/k_{y1}^2 \\ N_y &= \frac{A_3^2}{k_{y_3}^2} \\ T &= \left[\sqrt{\epsilon_{r_1}}M_xM_y + 2M_xN_y + 2N_xM_y\right. \\ &\quad \left. + 2\sqrt{\epsilon_{r_2}}Q_y(M_x + 2N_x)\right]^{-1} \end{aligned} \tag{11}$$

where

$$Q_y = \frac{A_4^2(2k_{y2}d + \mathrm{e}^{k_{y_2}d} - \mathrm{e}^{-k_{y_2}d})}{k_{y2}^2} \tag{12}$$

After that,

$$\begin{aligned} \alpha_c =& 4R_s\sqrt{\frac{\epsilon_0\beta}{\mu\beta_{h1}}}\frac{\epsilon_{r2}(M_x + 2N_x)T}{k_{y2}} \\ \alpha_d =& \frac{\omega}{2}\sqrt{\frac{\mu\epsilon_0\beta_{h1}}{\beta}}\left[(\tan\delta_1)\epsilon_{r1}M_xM_y + \right. \\ & \left. 2(\tan\delta_2)\epsilon_{r2}Q_y(M_x + 2N_x)\right]T \\ \alpha_r =& \left[M_xN_y + N_xM_y - 8R_s\sqrt{\frac{\epsilon_0\beta}{\mu\beta_{h1}}}\frac{\epsilon_{r2}N_x}{k_{y2}}\right. \\ & \left. -2\omega\sqrt{\frac{\mu\epsilon_0\beta_{h1}}{\beta}}(\tan\delta_2)\epsilon_{r2}N_xQ_y\right]T \\ \alpha =& \alpha_c + \alpha_d + \alpha_r \\ =& \left\{M_xN_y + N_xM_y + 4R_s\sqrt{\frac{\epsilon_0\beta}{\mu\beta_{h1}}}\frac{\epsilon_{r2}M_x}{k_{y2}}\right. \\ & + \frac{\omega}{2}\sqrt{\frac{\mu\epsilon_0\beta_{h1}}{\beta}}\left[(\tan\delta_1)\epsilon_{r1}M_xM_y\right. \\ & \left.\left. +2(\tan\delta_2)\epsilon_{r2}M_xQ_y\right]\right\}T \end{aligned} \tag{13}$$

where $\tan\delta_1$ and $\tan\delta_2$ are the loss tangents of the main dielectric and insular layer, respectively.

B. TE_{mn}^y Mode

According to the TM_{mn}^y mode, the characteristic equations for the TE_{mn}^y mode can be obtained in a similar format.

For the horizontal slab guides,

$$\begin{aligned} &1 + \frac{k_{y3}}{k_{y2}}\tanh(k_{y2}d/2) + \frac{k_{y3}}{k_{y1}}\tan(k_{y1}b/2) \\ &\quad -\frac{k_{y1}}{k_{y2}}\tanh(k_{y2}d/2)\tan(k_{y1}b/2) = 0, \quad \text{Region I} \end{aligned} \tag{14a}$$

$$1 - \frac{k_{y4}}{k_{y5}}\tan(k_{y_4}d/2) = 0, \quad \text{Regions II } \& \text{ III} \tag{14b}$$

where the defination of $k_{y1} \sim k_{y5}$ is the same as that in the TM_{mn}^y mode given by (2).

For the vertical slab guide,

$$1 + \frac{(\epsilon_{re1}k_{x0})^2 - (\epsilon_{re2}k_{x1})^2}{\epsilon_{re1}\epsilon_{re2}k_{x0}k_{x1}}\tan(k_{x1}a/2) - \tan^2(k_{x1}a/2) = 0 \tag{15}$$

which can then be split into

$$\begin{aligned} 1 + \frac{\epsilon_{re_1}k_{x0}}{\epsilon_{re_2}k_{x1}}\tan(k_{x1}a/2) = 0, \quad &\text{even mode} \\ 1 - \frac{\epsilon_{re_2}k_{x1}}{\epsilon_{re_1}k_{x0}}\tan(k_{x1}a/2) = 0, \quad &\text{odd mode} \end{aligned} \tag{16}$$

where the definition of ϵ_{re1}, ϵ_{re2}, k_{x0}, and k_{x1} is the same as that in the TM_{mn}^y mode given by (3) and (6).

Finally, by obtaining the mth root of k_{x1} through (15) and the nth root of k_{y1} through (14), the TE_{mn}^y mode is determined.

For brevity, the field components and attenuation constant, α, will not be listed here.

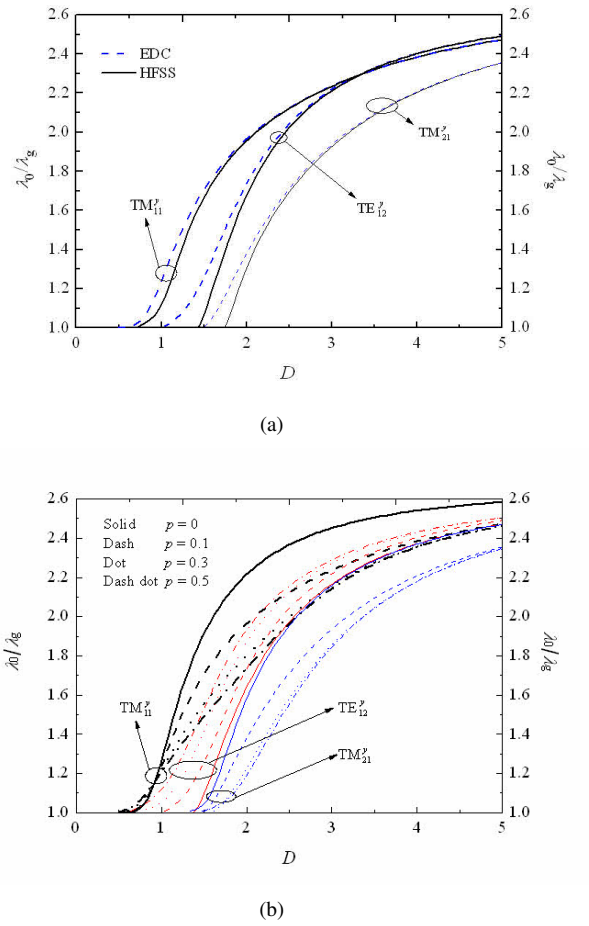

Fig. 2. The normalised guided wavelength vs. the normalised dimension D of the rectangular DIIG for $b/a = 1$: (a) comparisons among the EDC and FEM methods when $p = 0.1$, (b) various p's for the EDC method.

III. Calculation and Simulation

A rectangular DIIG with an aspect ratio of $b/a = 1$ is analysed, where various values of the insular ratio, $p = d/b$, are considered. The Dupont™ GreenTape™ 9K7 LTCC system is used as the dielectric material of the DIG, which has a relative dielectric constant, ϵ_r of 7.1 at 10 GHz. Its loss tangent is also characterised at 10 GHz to be $\tan\delta = 0.001$. The material used as the metallic ground plane here is copper plated on a RT/duroid 5880 board, which has a conductivity of $\sigma = 5.8\text{e}7$ S/m, a relative dielectric constant of 2.2 and a loss tangent of 0.001 at 10 GHz.

A. Phase Constant, β

Fig. 2 shows the normalised phase constant, β, as a function of the normalised dimension, D:

$$D = \frac{a+b}{\lambda_0}\sqrt{\epsilon_r - 1}. \tag{17}$$

In Fig. 2(a), the EDC and FEM methods are applied and compared for the case of $b/a = 1$ and $p = 0.1$. It can be seen that good agreement between the two methods is achieved for the three lowest-order modes.

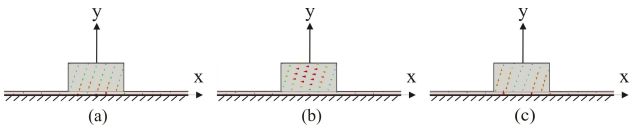

Fig. 3. The field distribution inside the DIIG of $b/a = 1$: (a) TM_{11}^y, (b) TE_{12}^y, (c) TM_{21}^y.

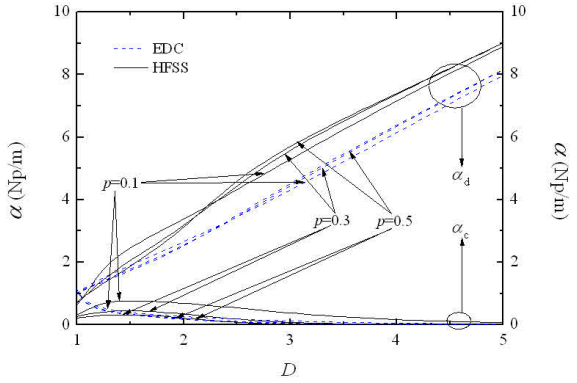

Fig. 4. The comparison between the EDC and FEM method in terms of the attenuation constant, α, of the TM_{11}^y mode vs. the normalised dimension, D, of the rectangular DIIG for $b/a = 1$.

In Fig. 2(b), the EDC method is applied to find out how different insular ratios may affect the propagating characteristics. As can be seen, the normalised guided wavelength, λ_0/λ_g which is equal to β/k_0, of the TM^y modes goes upward with the increase of p; while that of the TE^y modes does the opposite. This leads to a reduction in the single-mode bandwidth. So, the insular ratio, p, cannot be too large to maintain a reasonable single-mode bandwidth.

To provide a direct view of the field distribution within the cross-section of the DIIG, Fig. 3 shows three lowest-order modes for with an aspect ratio of $b/a = 1$ obtained through the rigorous FEM method. As the nomenclature of the DIIG modes follows that of the DG, the field variations in the y direction in Fig. 3 is in fact doubled, represented by n [4].

B. Attenuation Constant, α

The attenuation constant, α, of the fundamental TM_{11}^y mode is calculated here for the aspect ratio of $b/a = 1$ which exhibits the widest single-mode band. Both the EDC and FEM methods are employed.

Fig. 4 shows the calculated attenuation constant from the EDC and FEM methods in terms of α_d and α_c. A slowly-diminishing gap (about 10%) can be seen between two α_d's. In contrast, the agreement of α_c is much better.

Now the three constituent constants of α, α_d, α_c, and α_r are studied individually.

With the introduction of an insular layer, α_d decreases for all p's compared with that for $p = 0$ (the DIG). As far as the single-mode band of (normally $D < 2$) a transmission line is concerned, the higher p is, the lower α_d is..

The most obvious improvement from employing an insular layer is the significant reduction of the conductor loss, α_c, as

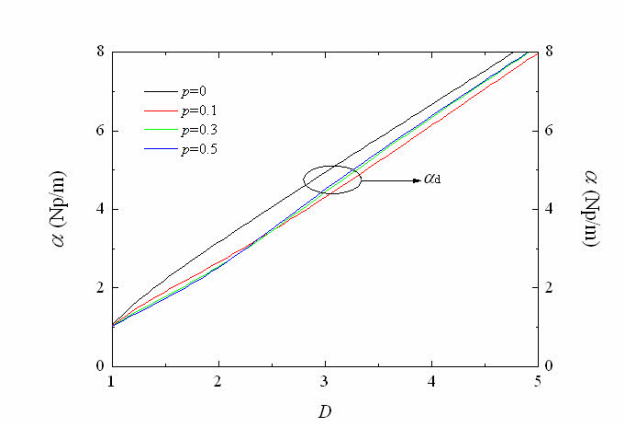

(a)

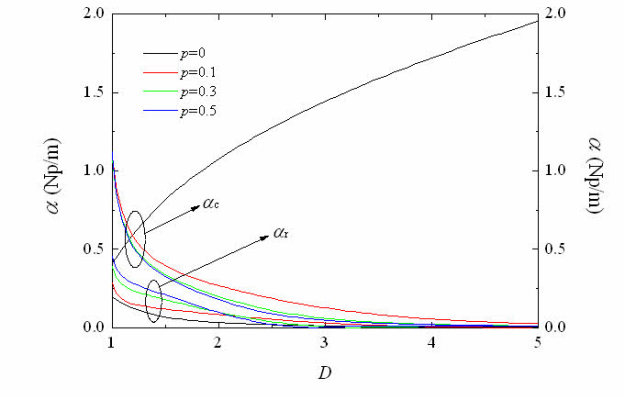

(b)

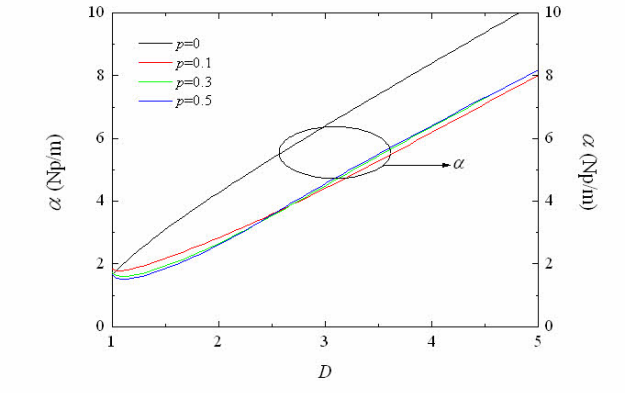

(c)

Fig. 5. The attenuation constant, α, of the TM_{11}^{y} mode vs. the normalised dimension, D, of the rectangular DIIG for $b/a = 1$: (a) α_d, (b) α_c and α_r, (c) α.

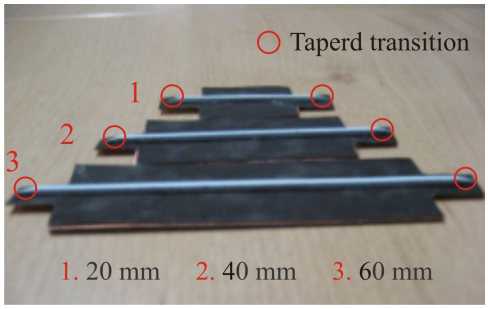

Fig. 6. Three fabricated DIIG samples of length 20 mm, 40 mm, and 60 mm.

observed in Fig. 5(b). For the DIG where $p = 0$, α_c increases with D; while for the DIIG, α_c decreases and tends to 0 at high D's. Furthermore, the higher p is, the lower α_c is. This is because the thicker the insular layer is, the more separation it creates. However, the radiation loss deteriorates for the DIIG. The reason for this is that the introduction of a low-permittivity dielectric loosens the confinement of electromagnetic fields and make them easily radiate. Since α_r is relatively low, the overall impact is not serious.

Finally, for the combination, α, significant reduction for all p's compared with the DIG can be observed in Fig. 5(c). In the single-mode band of the DIIG, a thicker insular layer will yield a lower loss.

IV. Measurement

Three dielectric rods with lengths of 20 mm, 40 mm, and 60 mm were fabricated using a standard LTCC technique and then assembled onto RT/duroid 5880 substrates to form DIIGs, as shown in Fig. 6. The Dupont™ GreenTape™ 9K7 LTCC system with a relative dielectric constant of 7.1 is employed as the dielectric, while the RT/duroid 5880 board, which has a relative dielectric constant of 2.2 and a thickness of 0.254 mm is adopted as the insular layer. Due to the restrictions of the LTCC technique, the thickness of the DIIG is chosen as 1.54 mm, formed from 7 layers of LTCC tape (0.22 mm for each layer after firing). So the insular ratio, p, is 0.16 which falls into the recommended range. To ensure the DIIG works in the Ka-band, the width of the DIIG is derived as 1.32 mm through the theoretical calculation.

As can be seen in Fig. 6, tapered transitions are added at both ends of the DIIG in order to be fed from a standard WR28. Note that the transitions are tapered in both horizontal and vertical planes to ensure a smooth transition.

Through the calibration technique introduced in [13], the propagation constant of the DIIG was extracted from the measured S-parameters of the three lines, and is illustrated in Fig. 7. The propagation constant simulated using HFSS is plotted in the same figure for comparison.

In Fig. 7, the measured phase constant, represented by the normalised guided wavelength, stays close to the simulated one, although it has some ripple. As for the measured loss constant, α, it is obviously higher than the simulated one, which indicates that the actual sample is more lossy. Possible reasons may lie in that the loss characteristics of the materials tend to be worse at higher frequencies and the bond between

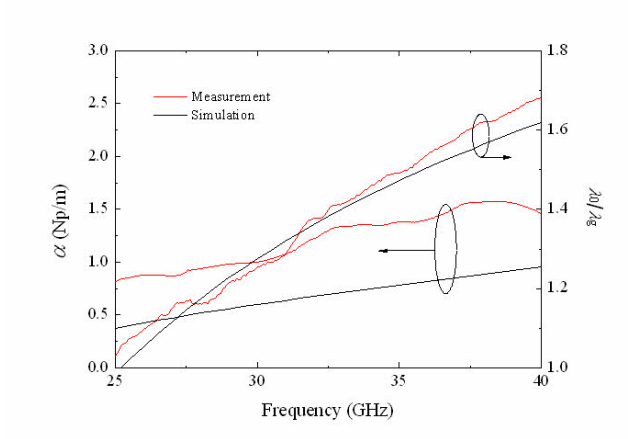

Fig. 7. Extracted propagation constant of the Ka band DIIG.

the LTCC and PCB board might not be perfect. Nevertheless, an α of 1.4 Np/m or 12.1 dB/m at 35 GHz is still an excellent loss performance.

V. Conclusion

Through the EDC method, a detailed theoretical analysis of the dielectric insular image guide (DIIG) has been presented. On one hand, the attenuation constant, α is significantly reduced by the introduction of the insular layer; on the other hand, the phase constant, β, of the fundamental and adjacent modes tend to get closer when the insular layer gets thicker, which narrows the single-mode bandwidth. The reduction of loss is, in fact, at the cost of a reduced single-mode bandwidth. This trade-off leads to a compromise of the insular ratio, p, with a recommended value between 0.1 and 0.3. The calculated results are compared with those from the rigorous FEM method and measurements. DIIGs comprising LTCC dielectric rods on RT Duroid substrate have been fabricated. Good agreement between theory and measurement has been demonstrated for the phase constant, β, and the attenuation constant of 12.1 dB/m at 35 GHz is an excellent loss performance. Further application of this analysis, and fabrication using other materials, can be expected to yield excellent results at higher frequencies, potentially even in the terahertz region.

Acknowledgment

The authors wish to acknowledge the financial support of the University of Leeds FIRS Scholarship scheme. Part of this work was sponsored by the Engineering and Physical Sciences Research Council (EPSRC) in the project ”3D Microwave and Millimetre-Wave System-on-Substrate using Sacrificial Layers for Printed MEMS components” in collaboration with Loughborough University and Imperial College London.

References

[1] S. K. Koul, Ed., *Millimeter Wave and Optical Dielectric Integrated Guides and Circuits*, 1st ed. Wiley-Interscience: New York, 1997.

[2] D. D. King, “Dielectric image lines,” *Journal of Applied Physics*, vol. 23, pp. 699 –700, Jun. 1952.

[3] R. Knox, “Dielectric waveguide microwave integrated circuits - an overview,” *Microwave Theory and Techniques, IEEE Transactions on*, vol. 24, no. 11, pp. 806 – 814, Nov. 1976.

[4] E. A. J. Marcatili, “Dielectric rectangular waveguide and directional coupler for integrated optics,” *Bell System Technical Journal*, vol. 48, pp. 2071 –2102, Sept. 1969.

[5] R. M. Knox and P. P. Toulios, “Integrated circuits for the millimeter through optical frequency range,” in *Proceedings of the Symposium on Submillimeter Waves*, Mar. 1970.

[6] S. Peng and A. Oliner, “Guidance and leakage properties of a class of open dielectric waveguides: Part i–mathematical formulations,” *Microwave Theory and Techniques, IEEE Transactions on*, vol. 29, no. 9, pp. 843–855, 1981.

[7] R. Mittra, Y.-L. Hou, and V. Jamnejad, “Analysis of open dielectric waveguides using mode-matching technique and variational methods,” *Microwave Theory and Techniques, IEEE Transactions on*, vol. 28, no. 1, pp. 36 – 43, Jan. 1980.

[8] J. E. Goell, “circular-harmonic computer analysis of rectangular dielectric waveguides,” *Bell System Technical Journal*, vol. 48, pp. 2133 – 2160, Sept. 1969.

[9] K. Ogusu, “Numerical analysis of the rectangular dielectric waveguide and its modifications,” *Microwave Theory and Techniques, IEEE Transactions on*, vol. 25, no. 11, pp. 874–885, 1977.

[10] M. Ikeuchi, H. Sawami, and H. Niki, “Analysis of open-type dielectric waveguides by the finite-element iterative method,” *Microwave Theory and Techniques, IEEE Transactions on*, vol. 29, no. 3, pp. 234 – 240, Mar. 1981.

[11] A. Oliner, S.-T. Peng, T.-I. Hsu, and A. Sanchez, “Guidance and leakage properties of a class of open dielectric waveguides: Part ii–new physical effects,” *Microwave Theory and Techniques, IEEE Transactions on*, vol. 29, no. 9, pp. 855 – 869, Sept. 1981.

[12] D. M. Pozar, *Microwave Engineering*, 3rd ed. Wiley India Pvt. Limited, 2009.

[13] F. Xu and K. Wu, “Guided-wave and leakage characteristics of substrate integrated waveguide,” *IEEE Transactions on Microwave Theory and Techniques*, vol. 53, pp. 66 – 73, 2005.

Lukui Jin (SM’12) received both his B.S. and M.S. degree in microwave engineering from Harbin Institute of Technology, Harbin, China, in 2008 and 2010, respectively. He is currently working toward the Ph.D. degree in the University of Leeds, Leeds, United Kingdom.

He is one of the 9 award holders of the prestigious Leeds Full-funded International Research Scholarship in 2010. His current research interests include design and analysis of substrate integrated waveguide, dielectric waveguide, and their applications in antennas and filters in the MCM technology.

Ian Robertson (M'96- SM' 05 -Fellow 12) was born in London in 1963. He received his BSc (Eng) and PhD degrees from King's College London in 1984 and 1990, respectively. From 1984 to 1986 he worked in the MMIC Research Group at Plessey Research (Caswell). After that he returned to King's College London, initially as a Research Assistant and then as a Lecturer, finally becoming Reader in 1994. In 1998 he was appointed Professor of Microwave Subsystems Engineering at the University of Surrey, where he established the Microwave Systems Research Group and was a founder member of the Advanced Technology Institute.

He has organized many colloquia, workshops, and short courses for both the IEE and IEEE. He was the Honorary Editor of IEE Proceedings - Microwaves, Antennas & Propagation for many years and Editor-in-Chief of the rebranded IET Microwaves, Antennas & Propagation from 2005 to 2009. He edited the book 'MMIC Design' published by the IEE in 1995 and co-edited the book RFIC & MMIC Design and Technology, published in English 2001 and in Chinese in 2007. He has published over 400 papers in the areas of MIC and MMIC design. In June 2004 he was appointed to the University of Leeds Centenary Chair in Microwave and Millimeter-Wave Circuits and he is now Head of the School of Electronic & Electrical Engineering.